Composites Part C: Open Access 14 (2024) 100450

Contents lists available at ScienceDirect

Composites Part C: Open Access

journal homepage: www.elsevier.com/locate/composites-part-c-open-access

A CAI study on transition zones of conventional and Double-Double laminates

Erik Kappel *, Yannick Boose, Mirko Mißbach

DLR, Institute of Composite Structures and Adaptive Systems, Lilienthalplatz 7, 38108 Braunschweig, Germany

ARTICLE INFO

Keywords:
Prepreg manufacturing
Single-sided diaphragm forming
Automated manufacturing

ABSTRACT

Laminate-thickness tapering opportunities of Double-Double (DD) laminates are unique, compared to conventional laminates (denoted as Quad) in aerospace, which are typically composed of 0°, 45°, −45°, 90° plies. The more aggressive tapering concept of DD, with drop-offs located on laminate's outer surfaces, promises simplification in terms of manufacturing. However, the DD concept bears the risk to impede crack propagation after impacts negatively, as no full plies cover building-block run outs.

The present article utilizes conventional CAI (AITM-1-0010) infrastructure to examine how the characteristics of DD and Quad laminates deviate, when laminate transition zones experience impact loads.

Sample dimensions and the overall testing procedure was executed as close as possible to the AITM norm, which is usually intended for testing quasi-isotropic, 4 mm thick laminates. The study focuses on M21E/IMA UD carbon-fiber epoxy prepreg.

A tapered sample represents the key object of the present experimental study. It features a laminate transition from 16- to a 32-ply region, with a 1:10 ramp. Both regions are quasi-isotropic. The individual ply run outs are distributed along the transition zone (staggering), as it is done in industry. The examined DD laminate represents a structural equivalent of the Quad laminate (identical $[A]$ matrix). The transition zone shows 4-building-block run outs.

The tapered samples are impacted from both sides, to assess the effects of the differences in laminate architecture. Constant-thickness, 16-ply and 32-ply, samples complement the tests of the tapered samples. The study features a delamination area assessment, based on ultra-sonic scans, as well as the analysis of CAI tests.

1. Motivation

The family of Double-Double (DD) laminates promises considerable simplifications compared to conventional laminates in aerospace used today. Those established laminates are denoted as Quad hereafter. They are usually composed of plies oriented in 0, 45, −45, 90°. Quad laminates are designed according to established guidelines in practice, as the symmetry requirement or the 10% rule. Those guidelines in combination with the pre-selected group of ply orientations limit the design space drastically. However, optimizing Quad laminates is still a challenging topic, as adjacent laminate zones need to be compatible to each other while laminate guidelines shall be fulfilled for each of the individual zones (see Figs. 1 and 2).

The symmetry requirement makes laminate-thickness tapering difficult, as two plies need to be dropped at once. The laminates' bending stiffness depends on the ply-stacking sequence. Optimizing the stacking sequence of a group of laminates is challenging as millions of conceivable combinations can exist, in particular when the laminate thickness and therefore the ply count increases.

The established rules allow for making save composite structures, which are in service for years in recent aircrafts. However, it is likely that pre-set angles as well as a group of design guidelines, whose origin are unclear sometimes, leave some space for improvement in terms of weight reduction or material-effort increase.

Double-Double laminates are proposed by Stephen W. Tsai [1] and co-workers to entrap hidden potentials of the group of CFRP materials. Likely DD will not outperform Quad laminates in all cases. However, the DD laminate family promises to simplify design processes, optimization, as well as manufacturing. Vermes et al. [2] provide a wide overview on the DD concept, with promising experimental and numerical analyses. A recent publication of Garofano et al. [3] presents a fuselage skin, optimized with DD in a crash context. The authors outline a considerable skin-weight reduction of 69.8%.

A DD laminate is described by $[\pm\Phi, \pm\Psi]_{rT}$. Φ and Ψ are ply-angles, r denotes the number of repeats and T denotes 'total' which is in line with Nettles [4]. Building blocks $[+\Phi, -\Psi, -\Phi, \Psi]$ are simply stacked on

* Corresponding author.
E-mail addresses: erik.kappel@dlr.de (E. Kappel), yannick.boose@dlr.de (Y. Boose), mirko.missbach@dlr.de (M. Mißbach).

https://doi.org/10.1016/j.jcomc.2024.100450
Received 24 January 2024; Received in revised form 29 February 2024; Accepted 29 February 2024
Available online 15 March 2024

Abbreviations

AFP	Automated-fiber-placement
AITM	AIRBUS test method
BB	4-ply building block (e.g. $[+\Phi, -\Psi, -\Phi, \Psi]$)
CAI	Compression after impact
CFRP	Carbon-fiber-reinforced-plastics
CLT	Classical laminate theory
Quad	Conventional laminate composed with 0°, 90°, +45° and −45° plies
DD	Double-Double
EEOP	Engineering edge of part
MEOP	Manufacturing edge of part
MRCC	Manufacturer's recommended cure cycle
UD	Unidirectionally (reinforced ply)

each other until the required laminate thickness is reached. A symmetry requirement does not exist. Thus, adjacent zones of a structure are all composed of the same BB, while the number of repeats can vary from zone-to-zone. The ply angles Φ and Ψ are identified based on the available load cases, as outlined in a previous publication [5]. Optimizing a DD structure is therefore similar to a sizing process for metal structures, in which the thickness is locally adapted. DD laminates optimization means finding the local number of repeats. In Quad laminates, tapering is realized by single-ply drop offs. Those drop offs are distributed in laminate-thickness direction and along a so called transition zone (staggering), which is typically defined by a ramp, as 1:10 or 1:20.

The basic DD concept differs (see Figs. 1 and 2). In a DD laminate full BBs are dropped of at once. According to the introducing DD literature drop offs can be located either on the parts tool or bag side. However, it shall be highlighted here that BB drop-off can also be located within the laminate stack. However, as four plies are dropped at once, resin pockets in the laminate architecture are the consequence, while their effect need investigation. The present study focuses on the 'bag-side' scenario, as it is considered the most promising setup for aerospace applications. Fig. 1 shows micro sections of both laminate architectures.

2. Experiment study

2.1. Impact testing

The present study distinguishes eight impact cases. Fig. 3 shows the four impact scenarios, which are executed for quad and DD laminates.

The AITM-1-0010 impact and compression fixture has been used for the study [6]. As the norm addresses testing of constant-thickness samples, the fixtures does not directly support testing of tapered samples. Therefore a compensation frame was made, to compensate the tapered bag-side surface of the ramp-down samples (case 4 in Fig. 3). With the frame in place the perpendicularity of the impact event on the tool-side of the sample is assured. The frame is also used during compression testing, to create the line-like contact along the sample length. The frame is shown in Fig. 4. It is made by 3D printing from PA12.

It shall be highlighted that the frame affects the impact procedure slightly. It lifts the impacted surface of the sample by measured 4.43 mm. The ramp-down samples were all tested with 50 J impact energy, which is equivalent to 1003 mm travel, with an impactor velocity of 4.31 m/s at the first contact. This frame shifts the impact accident slightly, by

$$t_{shift} = \frac{4.427 \cdot \text{mm s}}{4.31 \text{ m}} = 1.03 \text{ ms} \quad . \tag{1}$$

The corresponding reduction of the travel length due to the frame reduces the effective impact energy. The effect can be estimated to an effective impact energy of

$$\frac{50 \text{ J}}{1003 \text{ mm}} = \frac{x}{998.57 \text{ mm}} \quad \rightarrow \quad x = 49.78 \text{ J} \quad . \tag{2}$$

This represents a deviation of −0.44%. Fig. 5 shows how the frame is used for the impact test of the ramp-down configuration.

2.2. Sample manufacturing

All samples in this study are made from Hexcel's medium grade M21E/IMA UD prepreg, with a nominal ply thickness of 0.184 mm. Note, that Wang et al. [7] and Caminero et al. [8] examine CAI for the same prepreg material.

All samples were manufactured in a single autoclave run, with a single two-hour dwell stage curing cycle, with 180°C curing temperature. Fig. 6 shows the uncured laminates prior the vacuum bagging assembly. The CFRP samples were made on a flat steel tool in a single-sided process. The final samples were cut to the 150 mm × 100 mm dimensions of the AITM norm.

The tapered samples feature a laminate-thickness transition zone from 16 to 32 plies, equivalent to 2.94 mm to 5.88 mm laminate thickness. A 1:10 ramp has been realized for the samples at hand, leading to a transition-zone length of 29.4 mm. Fig. 7 shows the cross section of a tapered sample, with EEOP and MEOP denoting the engineering- and manufacturing-edge-of-part respectively.

The AITM norm suggests to use quasi-isotropic laminates (see page 5 in [6]). Thus, the tapered Quad samples start with the thin, 16-ply stacking $[-45, 90, 45, 90, 45, 0, -45, 0]_s$ and end with the thick 32-ply section: $[[-45, 90, 45, 0]_{2s}]_s$, which is in line with Gaarstka [9] . Fig. 8 shows

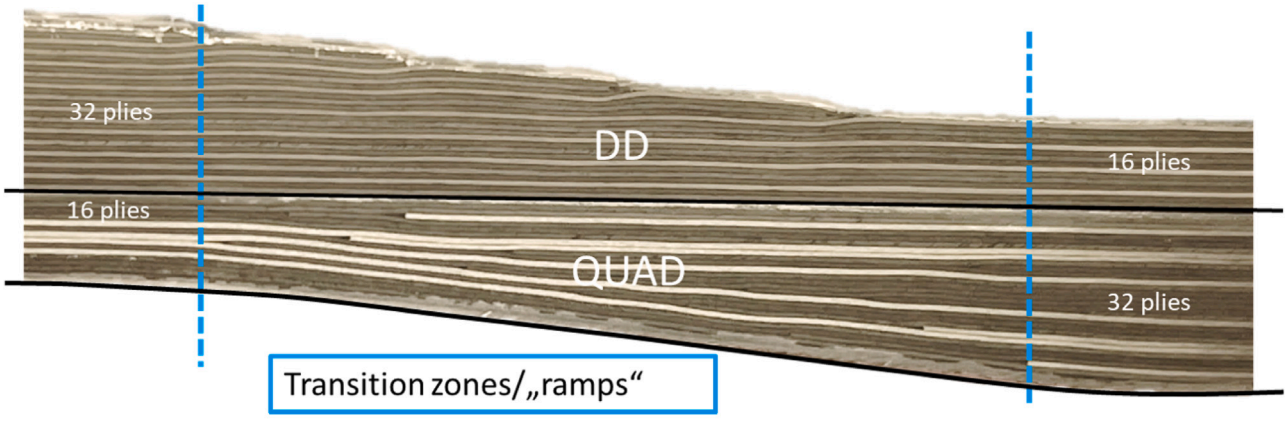

Fig. 1. Laminate architecture in ramps.

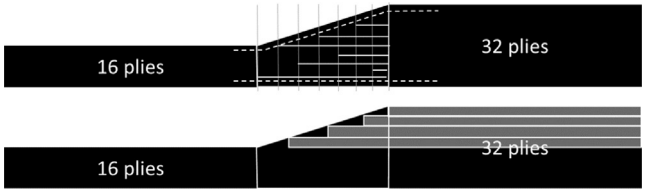

Fig. 2. Laminate architecture.

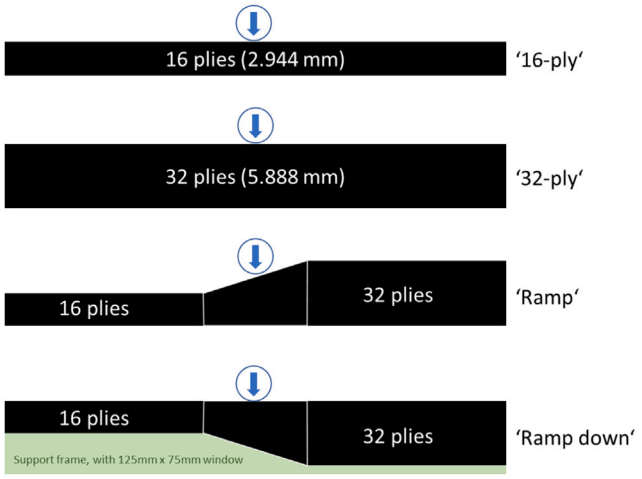

Fig. 3. Impact configurations with corresponding sample names, respectively.

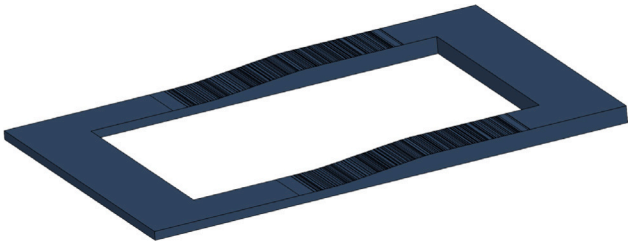

Fig. 4. Frame for clamping purposes, compensating the tapered bag-side.

Fig. 5. Frame in AITM fixture.

how the ply-drop offs are distributed in laminate-thickness direction and along the transition zone.

The tapered DD samples use the $[22.5, -22.5, 67.5, -67.5]$ building block, which can also be considered a $[0, -45, 45, 90]$ sub-laminate rotated by 22.5°. The thickness-normalized in-plane stiffness $[A^*]$ is identical for DD and Quad, as outlined hereafter for the examined prepreg (material data in Table 2 in Appendix).

$$[A^*]_{Quad} = [A^*]_{DD} = \begin{bmatrix} 64201.1 & 20597.2 & 0.0 \\ 20597.2 & 64201.1 & 0.0 \\ 0.0 & 0.0 & 21802.0 \end{bmatrix} \frac{\mathrm{N}}{\mathrm{mm}^2}$$

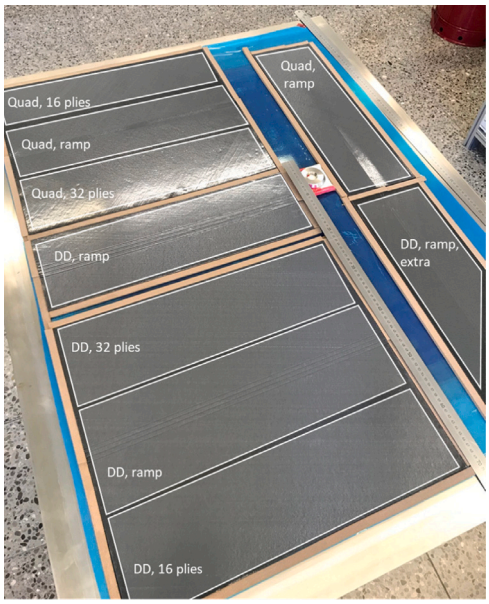

Fig. 6. Sample manufacturing.

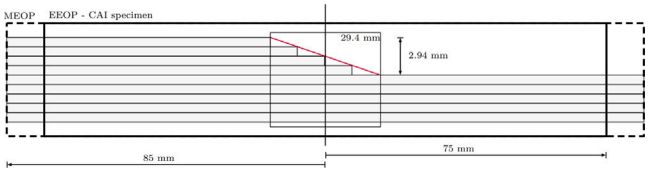

Fig. 7. Ramp specimens.

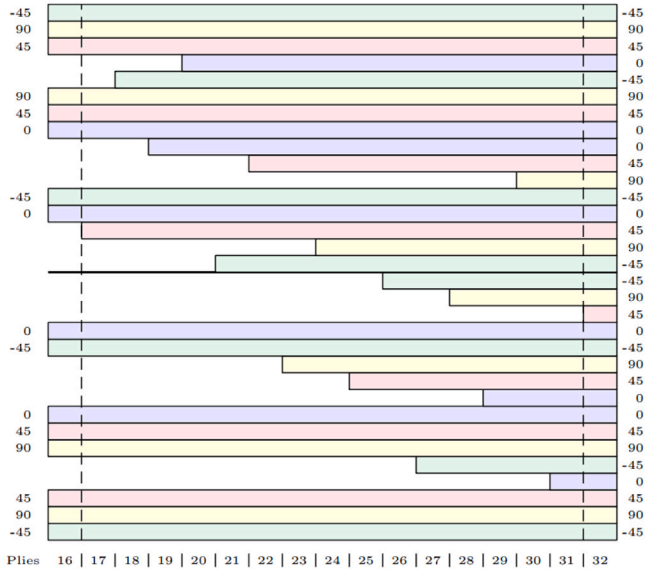

Fig. 8. Laminate stacking details in QUAD ramp. Thin 16-ply section: $[-45, 90, 45, 90, 45, 0, -45, 0]_s$, Thick 32-ply section: $[[-45, 90, 45, 0]_{2s}]_s$.

The thin laminate region is composed of four BBs, while the thick region consist of eight. The transition features four discrete steps, as indicated in Fig. 7.

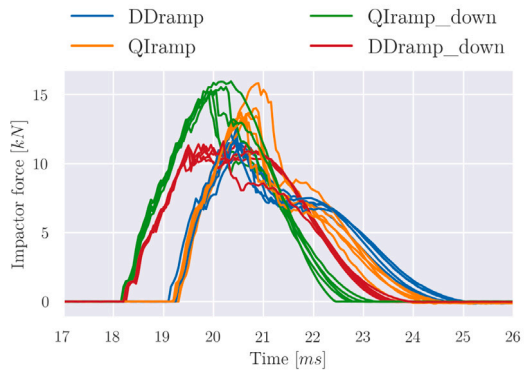

(a) Force-over-time

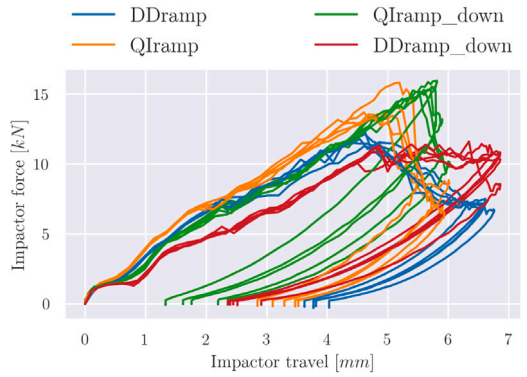

(b) Force-over-travel

Fig. 9. Impactor data for ramped samples. (QI = Quad).

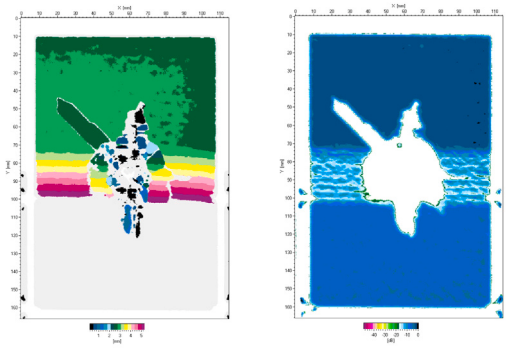

(a) Quad - delam. depth (b) Quad - total delam.

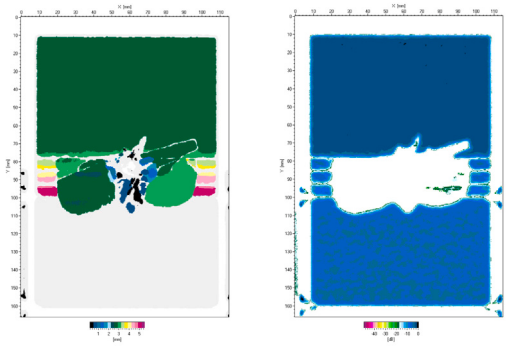

(c) DD - delam. depth (d) DD - total delam.

Fig. 10. Example results for Quad ramp-down sample (top row) and DD Ramp-down sample (bottom row) and specific evaluation results.

3. Impact study

40 samples are examined in the present study. A two-path strategy is pursued, defined by:

- Constant-thickness laminates are tested at five individual impact-energy levels. This procedure was executed for DD and Quad to check for remarkable deviations between both laminate types, while keeping testing efforts moderate.
- The tapered configurations were all tested with fives samples each. All tapered samples were tested with 50 J impact energy, which was deduced from the 32-ply tests as a reasonable impact energy.

3.1. Impact assessment

Fig. 9 shows impactor forces along the impact-test duration and the corresponding impactor travel. Fig. 9(a) substantiates the outlines effect of the frame, leading to a little shift of the impact incident.

The plot characteristics a very similar for all configurations. The characteristics match results presented by Rivallant et al. [10], Aoki et al. [11] or Duan et al. [12]. The Quad samples show higher impact-force maxima. The impactor force over impactor travel graph shows a similar linear trend. Only the DD ramp_down sample shows a slightly lower impactor force inclination.

3.2. US scan analysis

Ultrasonic scans are used to assess delamination areas after the impacts, as it is required by the AITM norm. Different scanning techniques were used, while two are described hereafter.

- For visualizing the delamination depths a time-of-flight or intermediate-echo technique has been used. These results are denoted as ‘delam. depth’ hereafter
- For visualizing the total delamination area the reflector-echo technique has been used. These results are denoted as ‘total delam.’ hereafter.

Fig. 10 shows example results for both evaluation techniques for ramp samples (DD and Quad), both impacted with 50 J.

The delamination depth analysis is impeded by thickness tapering, as can be seen in Figs. 10(a), 10(c). In addition, surface-close delaminations mask laminate regions underneath which makes an in-depth characterization underneath a surface delamination impossible. CT analysis are more suited for this kind of analysis, as performed by Cunha et al. [13]. Thus, the following delamination-area assessment use the ‘total delam’ results. A Python-based framework has been set up to provide a user independent assessment tool to quantify delamination areas of the impacted samples. The framework is based on OpenCV functionalities, It basically identifies the outer contour of the delamination areas. The contour information is used to

- quantify the total delamination area and the damage fraction of the whole sample
- define a hull-type, sample-edge-parallel rectangle, whose dimensions refer to delamination width and height.

Fig. 11 shows the example results for both samples from Fig. 10.

3.3. Critical remark

The developed delamination assessment tool automatically quantifies the delamination area and the dimensions of a sample-edge-parallel delamination-circumscribing rectangle. The rectangle’s width is used to

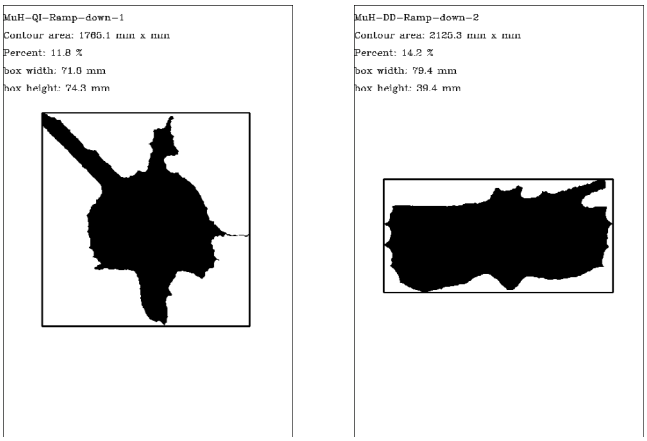

(a) Quad result (b) DD result

Fig. 11. Delamination assessment results, determined with the realized Python framework.

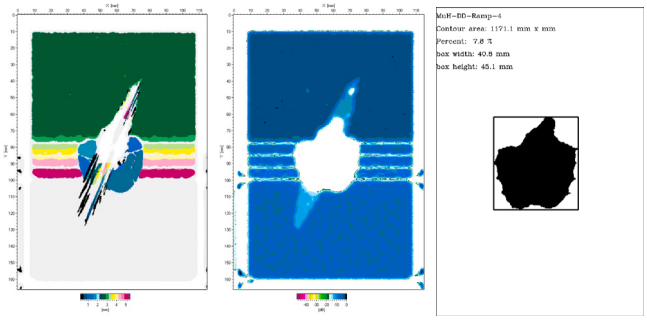

Fig. 12. US scan issue for DD-ramp samples.

quantify the total damage width, which affect the relevant cross section during the compression test. The python tool identifies and ranks closed contours from the bluish total-delamination plots. Finally, the largest white contour is quantified. This user-independent procedure works well for the majority of samples. However, for tapered DD ramp samples, an issue has been observed, which is linked to the US scan generation procedure. Fig. 12 outlines the issue for the DD-ramp sample

As the malfunction was observed after finalizing the compression tests, repeating the US scans could not be executed. The observed discrepancy, in linked to out-of-plane fiber-tearing, which is shown in Fig. 13(b) for the affected DD-ramp samples. Table 1 summarizes all US scan analysis, relating impact energies with delamination widht and the total delamination area.

3.4. Visual observations

Images of the tested CAI samples are presented hereafter, allowing for differentiation between both laminate families. Fig. 13 shows the ramp samples. Fig. 14 shows the ramp-down samples. All shown samples are tested with 50J impact.

- Both laminate families show reproducible delamination patterns
- Delamination shapes differ completely between DD and Quad.
- Delamination patterns are controlled by certain ply orientations for both laminate types, as can be seen in Fig. 10.

- **Ramp samples:** The Quad laminates show surface cracks along the 0° direction on the impacted side passing through the impactor dent. The DD samples show no surface cracks on the impacted side (see Fig. 13(a)).

Table 1
Summary of delamination assessments for all tested samples. Delamination areas for *-marked samples erroneous(see Section 3.3)

ID	Impact J	Delam. width mm	Delam. area mm^2
DD-16–1	20	19.4	224.63
DD-16–2	15	14.5	137.13
DD-16–3	30	34.1	408.28
DD-16–4	25	21.2	263.99
DD-16–5	35	28.0	297.91
DD-32-1 *	50	31.4	967.72
DD-32-2 *	55	31.6	871.21
DD-32-3 *	60	39.6	1045.02
DD-32-4 *	65	34.1	1022.77
DD-32-5 *	72	44.9	1760.04
DD-Ramp-1	50	37.1	872.93
DD-Ramp-2	50	35.7	891.92
DD-Ramp-3	50	38.6	975.07
DD-Ramp-4	50	40.8	1171.05
DD-Ramp-5	50	34.1	796.76
DD-Ramp-down-1	50	77.8	1546.94
DD-Ramp-down-2	50	79.4	2125.29
DD-Ramp-down-3	50	75.5	1684.45
DD-Ramp-down-4	50	76.1	1831.92
DD-Ramp-down-5	50	77.8	1679.03
QI-16–1	15	18.2	223.73
QI-16–2	20	22.9	402.67
QI-16–3	25	23.1	545.16
QI-16–4	30	28.8	635.65
QI-16–5	35	45.7	1020.09
QI-32–1	72	47.3	2469.63
QI-32–2	65	33.7	1091.30
QI-32–3	60	41.4	1333.83
QI-32–4	55	40.0	1412.37
QI-32–5	50	37.6	934.99
QI-Ramp-1	50	47.1	1057.15
QI-Ramp-2	50	56.1	1755.28
QI-Ramp-3	50	58.2	2098.03
QI-Ramp-4	50	65.1	1329.22
QI-Ramp-5	50	42.7	1280.33
QI-Ramp-down-1	50	71.8	1765.10
QI-Ramp-down-2	50	41.8	1401.48
QI-Ramp-down-3	50	41.4	1595.56
QI-Ramp-down-4	50	45.9	1794.23
QI-Ramp-down-5	50	67.8	1639.18

- **Ramp samples:** The backside views show similar damage characteristics. One finds dominance of the 22.5° ply for DD and −45° for Quad. As the damage follows the ply alignment, the determined damage width is higher for the Quad samples.

Fig. 14 outlines the ramp-down samples.

- **Ramp-down samples:** The Quad laminates show cracks along the 0° direction on the impacted sides, passing through the impactor dent. The DD laminates show smaller bifurcated cracks, aligned along the 22.5° direction and perpendicular
- **Ramp-down samples:** The Quad samples show fiber tearing on the opposite surface across the ramp region, which is aligned along the −45° direction. The DD samples show fiber tearing at the thin laminate region, aligned along the 67.5° direction. The tearing does not migrate into the steps of the ramp region on the surface. However, photo 14(a) indicates some migration damage underneath the BB run outs.

Fig. 15 summarizes the test of the 16- and 32-ply constant-thickness samples.

The samples show the same surface-crack patterns, which were identified for the tapered samples. Quad samples show a straight crack along the 0° direction. DD sample show bifurcated cracks around the impactor dent, with crack directions following the ply orientations.

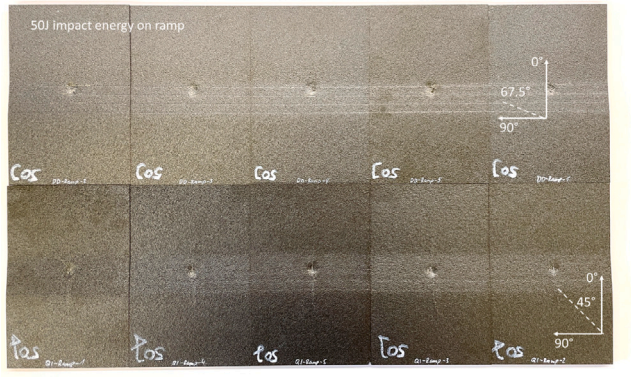

(a) Impact on ramp (top view)

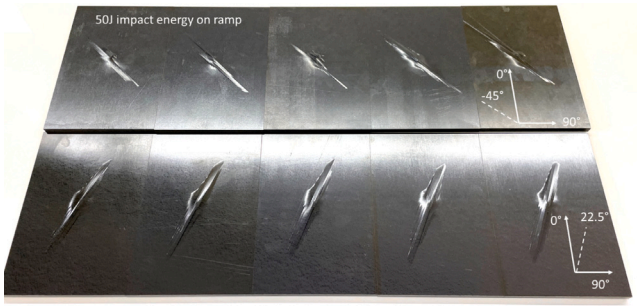

(b) Bottom view

Fig. 13. Ramp samples.

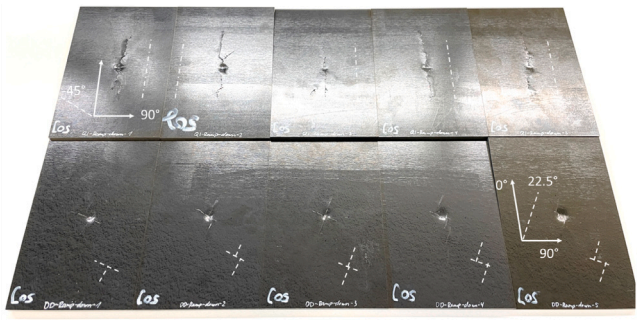

(a) Impacted side

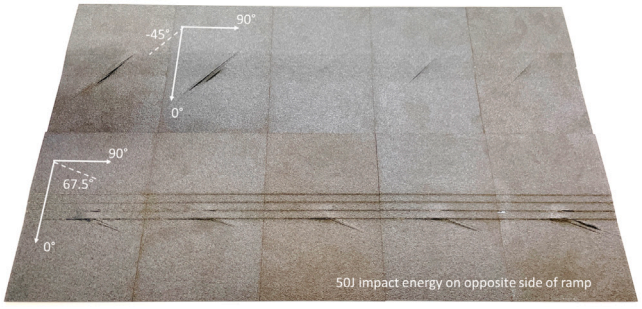

(b) Opposite side

Fig. 14. Ramp-down samples.

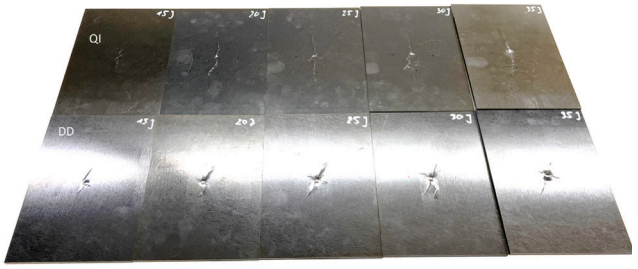

(a) 16-ply

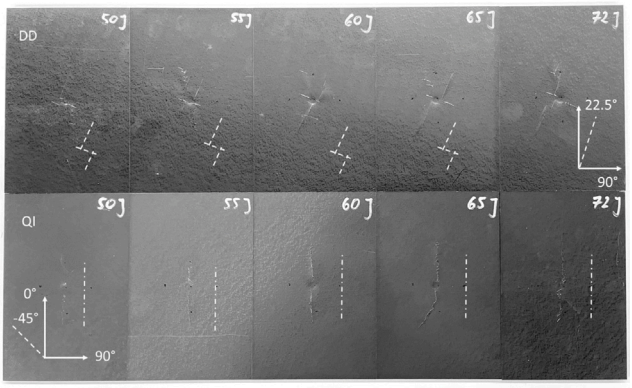

(b) 32-ply

Fig. 15. Constant-thickness samples.

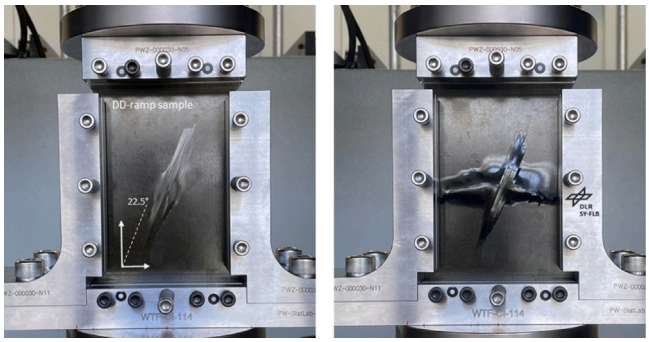

Fig. 16. Compression test of a DD-ramp sample.

4. Results

4.1. Compression testing

In the AITM-1-0010 norm, the 'typical sample would be quasi-isotropic and approximately 4.0 mm thick'. The compression strength for a certain impact-energy level (E) is quantified based on the break failure load (P_r) and the samples' rectangular cross section, described by the sample width (w) and the measured sample thickness (t).

$$\sigma_r(E) = \frac{P_r}{w \cdot t} \tag{3}$$

This definition can be applied for the 16- and 32-ply sample of the present study. However, the definition is not meaningful for the tapered samples examined here, as the effective sample thickness varies along

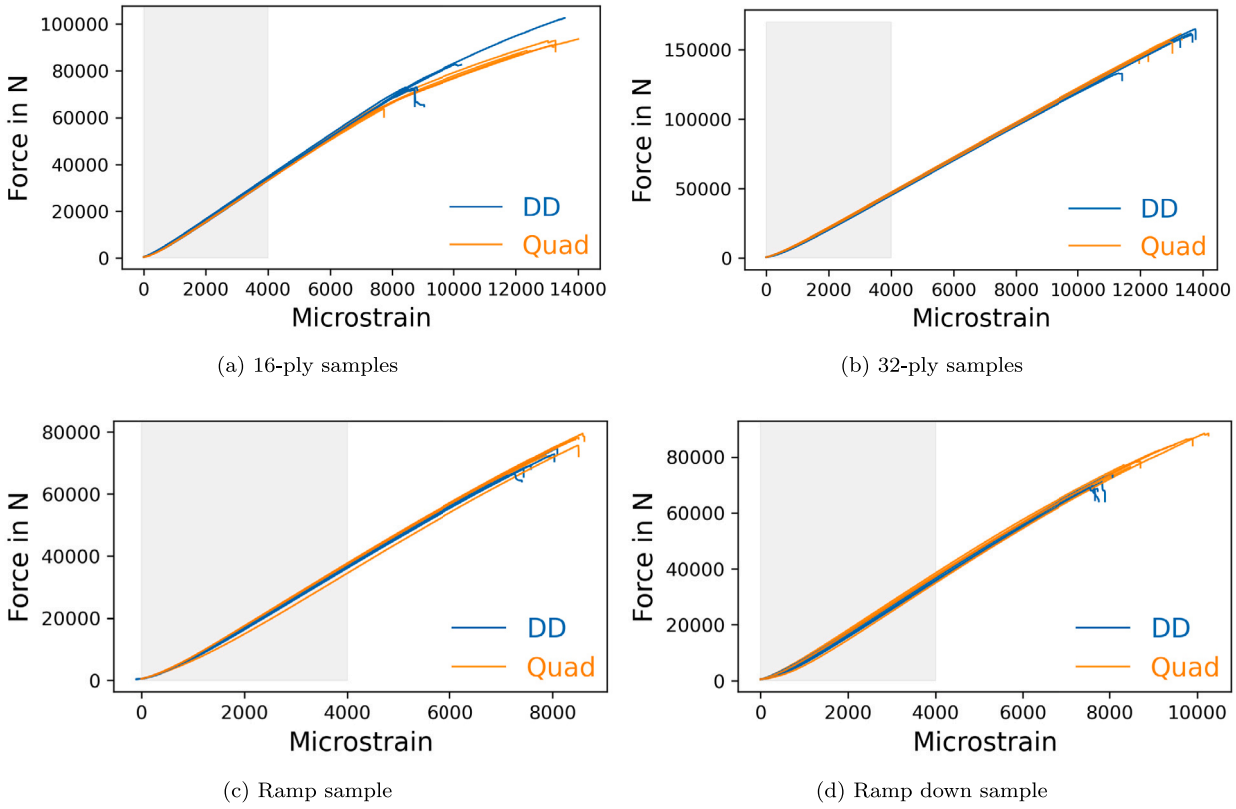

Fig. 17. Compression tests of impacted ramp down and ramp samples.

the transition zone. Therefore, the following analyses refer to the samples' break load P_r.

'Typical maximum strain values used in design are between 4000–5000 microstrain in tension and 3000–4000 microstrain in compression', can be found in Baker et al. [14].

Fig. 17 shows the Force-over-strain graphs of all impacted configurations. Force and strain are plotted positive for illustration purposes, even though the graphs refer to the compression load case (see Figs. 16, 18 and 20).

The graphs reveal no conspicuous artifacts. Neither bifurcation nor strong non linearity are observed, which usually indicates buckling. Only, the 16-ply Quad configuration shows a little non linearity after passing 5000 microstrain compression.

Thus, the tests substantiate the identical laminate stiffness (DD vs. Quad), which is indicated by the identical $[A^*]$ matrices (see Table 3).

Fig. 19 shows all determined force-strain graphs and the theoretical graphs for intact 100 mm wide 16- and 32-ply samples. The latter are determined using $\varepsilon_x = a_{11} \cdot N_x$, with a_{11} being the first entry of the inverted laminate-stiffness matrix $[a] = [A]^{-1} = (t_{lam} \cdot [A^*])^{-1}$ from CLT.

5. Conclusion

The nominally identical laminate-stiffness properties of the examined Quad and DD laminates is found present after the samples have been impacted. Breakage loads differ, with advantageous for the Quad family, but up to 7000 microstrain compression strain show identical stiffness (Force-vs-strain).

High level assessment:

- Delamination characteristics are reproducible for each laminate family.
- Delamination pattern differ completely between QUAD and DD
- Both laminate families show similar scattering of break loads
- DD ramp-down sample show higher damage width than the Quad, which correlates with lower break-load values
- QUAD and DD sample show reproducible damages around the impactor contact region.
  - QUAD laminates shows cracks along the 0° direction of the samples, which is aligned parallel to the long edge of the CAI sample. The crack orientation does not correlate with the outermost UD plies in the laminate stack.
  - DD samples show bifurcated crack patterns around the impactor contact region. Cracks migrate parallel and perpendicular to the outermost ply orientation.
  - Constant-thickness, 16- and 32-ply sample shows representative crack patterns, whose propagation range increases with increasing impact energy. Remarkable changes were not observed for the tested range of 15–35 J (16-ply samples, 2.94 mm) and 50–72 J (32-ply samples, 5.88 mm)
- Impacting the ramp regions induces fiber tearing on the samples backside.

Fig. 21 summarize the delamination areas of the tapered samples.

The DD ramp-down samples show a remarkable characteristic of the delamination pattern. The delamination areas are found comparably wide in the samples width direction. The ramp samples, in contrast, do not show similar differences between DD and Quad. Recalling Fig. 14(a), indicates that the delamination develops between the 4-building-block base laminate and the ramped laminates portion. Even though it is contrary to DD's initial concepts, it could be beneficial to distribute the base laminate, with two one-half acting as cover laminate.

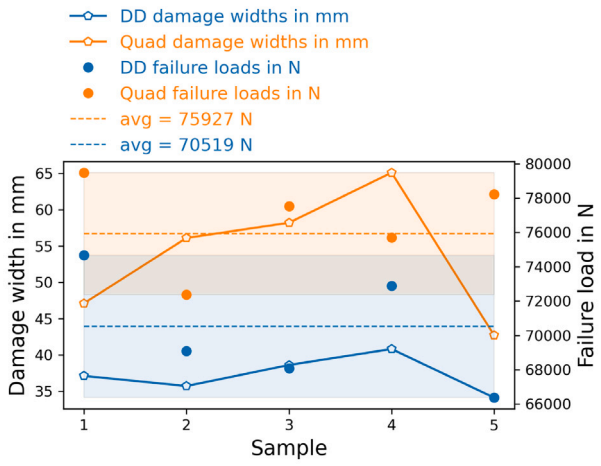

(a) Ramp samples

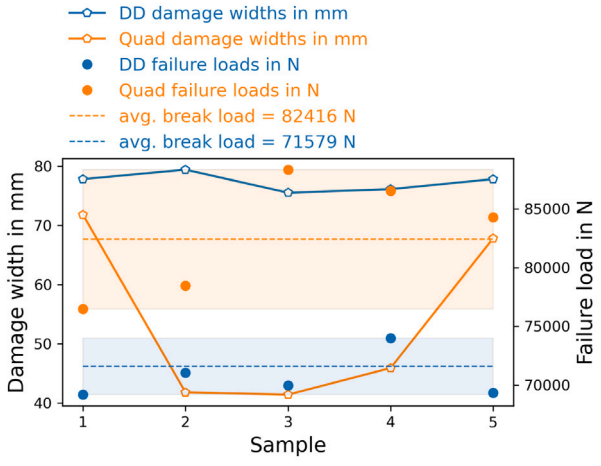

(b) Ramp-down samples

Fig. 18. Damage widths and failure loads for tapered samples.

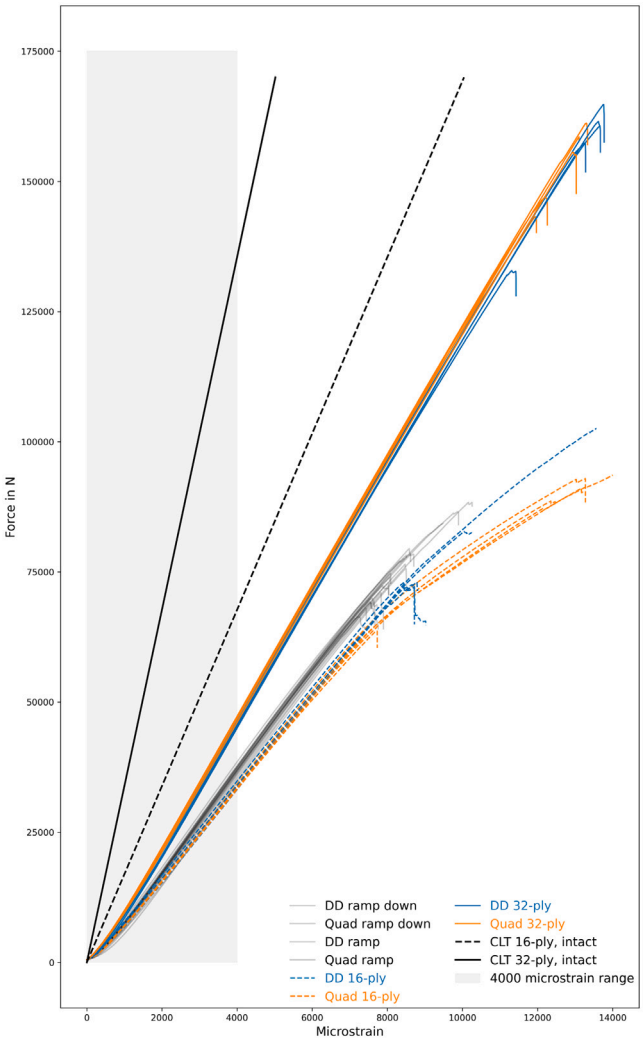

Fig. 19. Ramped samples (gray), 16-ply and 32-ply samples.

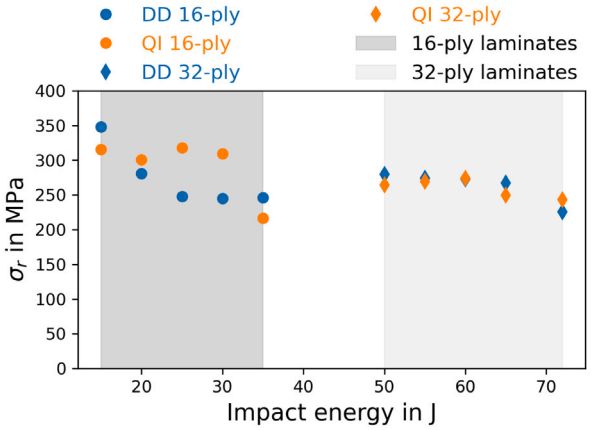

Fig. 20. Constant-thickness 16-ply and 32-ply samples.

CRediT authorship contribution statement

Erik Kappel: Writing – original draft, Visualization, Validation, Methodology, Investigation, Formal analysis, Data curation, Conceptualization. **Yannick Boose:** Investigation, Conceptualization. **Mirko Mißbach:** Writing – review & editing, Investigation, Conceptualization.

Declaration of competing interest

The authors declare that they have no known competing financial interests or personal relationships that could have appeared to influence the work reported in this paper.

Data availability

The data that has been used is confidential.

Acknowledgments

The research leading to these results has received funding from the German Federal Ministry for Economics and Climate Action (BMWK) under project number 20A2103C (MuStHaF-DLR) .

Appendix

A.1. Sample properties

See Table 2.

(a) Ramp samples

(b) Ramp-down samples

Fig. 21. Total delaminations of tapered samples. Top rows refer to DD laminates. All samples tested with 50 J.

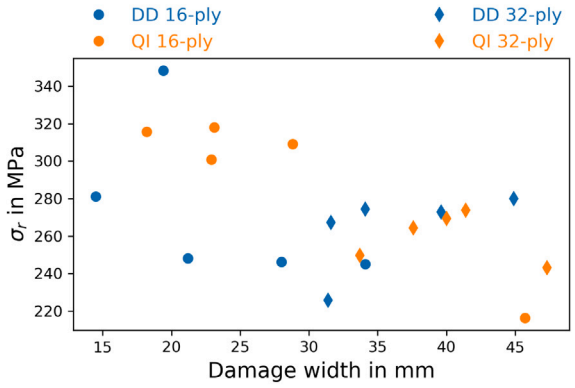

(a) Damage width correlation

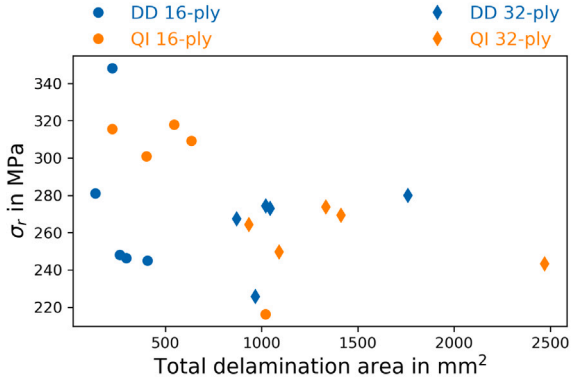

(b) Damage area correlation

Fig. 22. Strength vs. damage with and total delamination area.

Table 2
Material parameters M21E/IMA.
Source: From [7]

E_1	Longitudinal modulus	154.0 GPa
E_2	Transverse modulus	8.5 GPa
G_{12}	In-plane shear modulus	4.2 GPa
ν_{12}	Poisson ratio	0.35
t_{ply}	Ply thickness	0.184 mm

A.2. Constant-thickness samples

See Figs. 22 and 23.

A.3. Reflector-echo technique results

See Figs. 24–31.

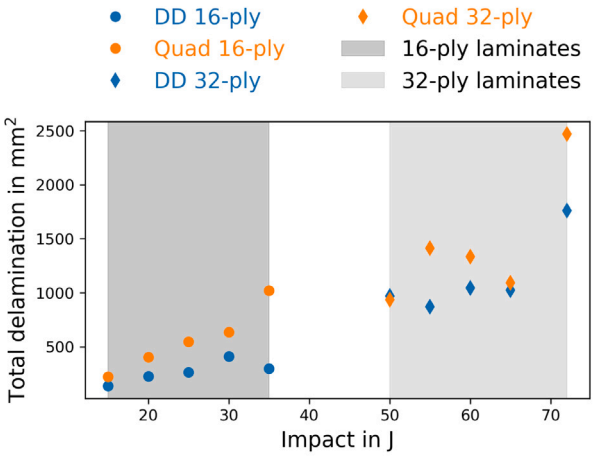

(a) area over impact

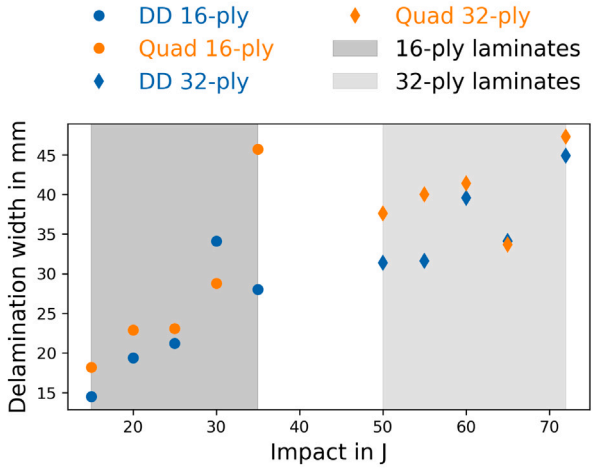

(b) damage width over impact

Fig. 23. Correlation Delamination width and area over impact energy.

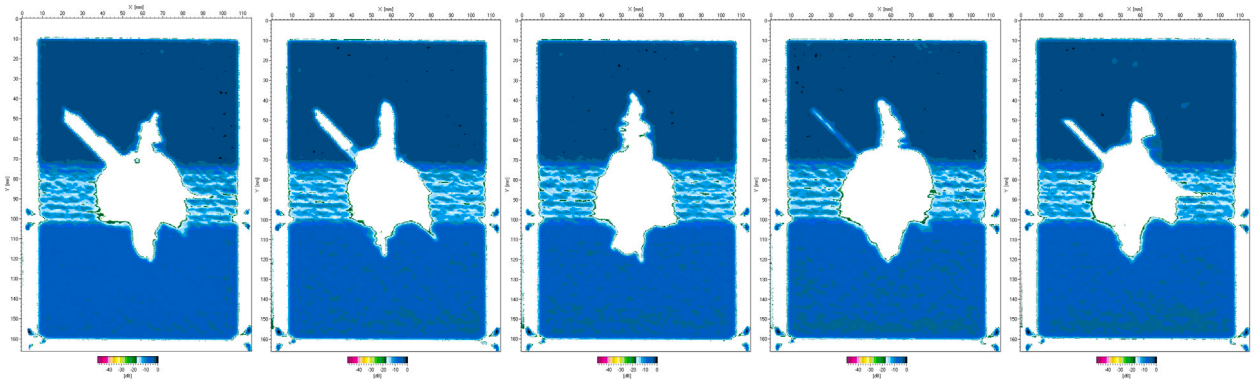

(a) 50 J (b) 50 J (c) 50 J (d) 50 J (e) 50 J

Fig. 24. Reflector-echo results for QI ramp down.

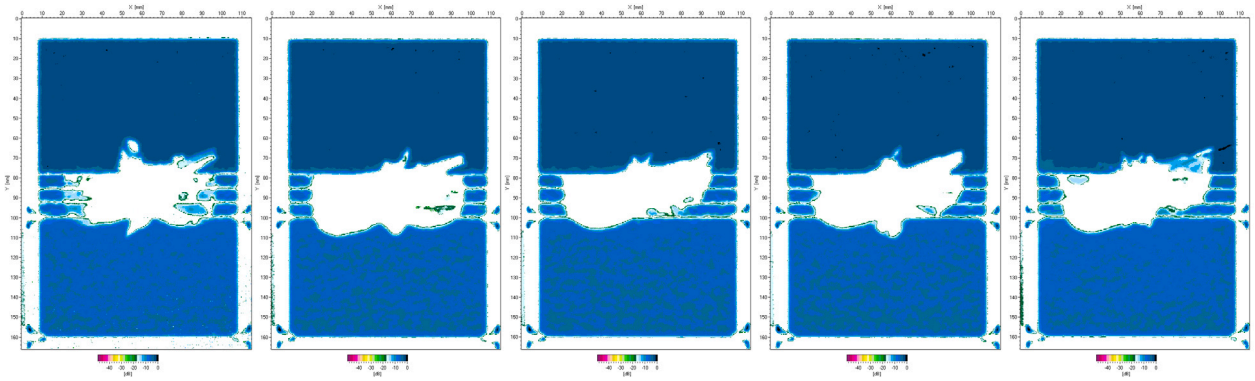

(a) 50 J (b) 50 J (c) 50 J (d) 50 J (e) 50 J

Fig. 25. Reflector-echo results for DD ramp down.

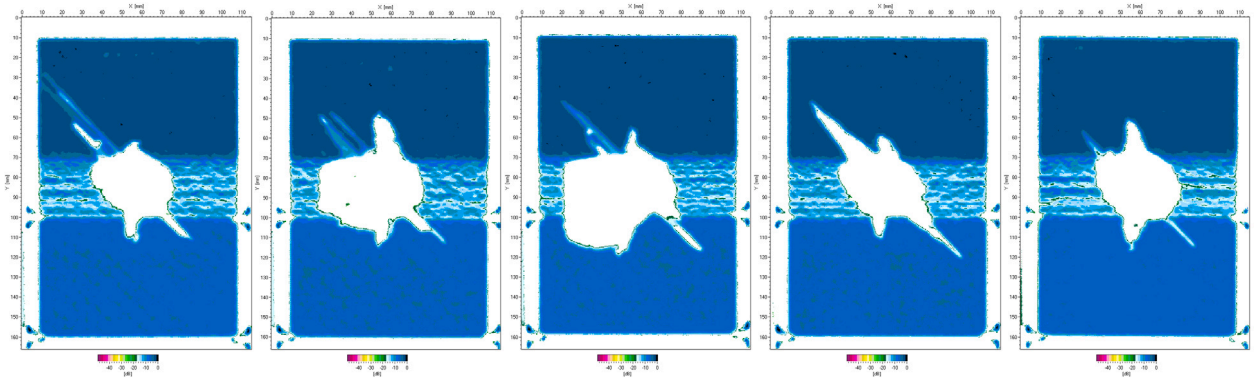

(a) 50 J (b) 50 J (c) 50 J (d) 50 J (e) 50 J

Fig. 26. Reflector-echo results for QI ramp.

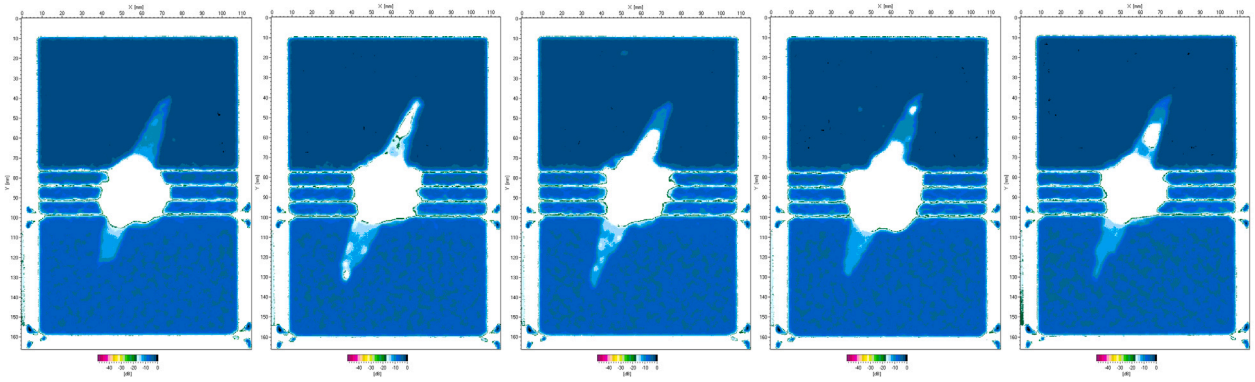

(a) 50 J (b) 50 J (c) 50 J (d) 50 J (e) 50 J

Fig. 27. Reflector-echo results for DD ramp.

Table 3
Samples' normalized stiffness and bending-stiffness matrices.

ID	Plies	Nominal thickness	$[A^*]$ in N/mm^2	$[D^*]$ in N/mm^2
Quad thin	16	2.94	$\begin{bmatrix} 64201.1 & 20597.2 & 0.0 \\ 20597.2 & 64201.1 & 0.0 \\ 0.0 & 0.0 & 21802.0 \end{bmatrix}$	$\begin{bmatrix} 36867.2 & 23897.6 & -3433.4 \\ 23897.6 & 84934.4 & -3433.4 \\ -3433.4 & -3433.4 & 25102.3 \end{bmatrix}$
Quad thick	32	5.89	$\begin{bmatrix} 64201.1 & 20597.2 & 0.0 \\ 20597.2 & 64201.1 & 0.0 \\ 0.0 & 0.0 & 21802.0 \end{bmatrix}$	$\begin{bmatrix} 60371.8 & 21422.3 & -1931.3 \\ 21422.3 & 66380.2 & -1931.3 \\ -1931.3 & -1931.3 & 22627.1 \end{bmatrix}$
DD thin	16	2.94	$\begin{bmatrix} 64201.1 & 20597.2 & 0.0 \\ 20597.2 & 64201.1 & 0.0 \\ 0.0 & 0.0 & 21802.0 \end{bmatrix}$	$\begin{bmatrix} 64201.1 & 20597.2 & 825.1 \\ 20597.2 & 64201.1 & -825.1 \\ 825.1 & -825.1 & 21802.0 \end{bmatrix}$
DD thick	32	5.89	$\begin{bmatrix} 64201.1 & 20597.2 & 0.0 \\ 20597.2 & 64201.1 & 0.0 \\ 0.0 & 0.0 & 21802.0 \end{bmatrix}$	$\begin{bmatrix} 64201.1 & 20597.2 & 206.3 \\ 20597.2 & 64201.1 & -206.3 \\ 206.3 & -206.3 & 21802.0 \end{bmatrix}$

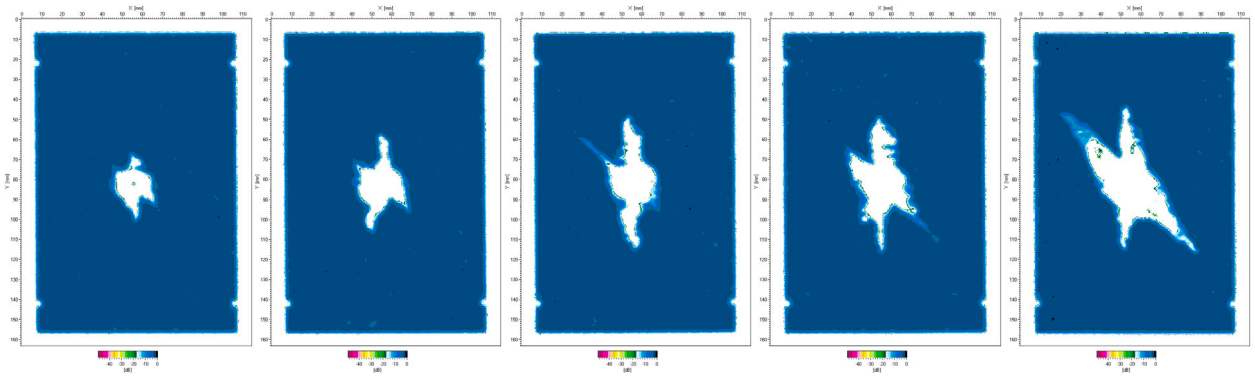

(a) 15 J (b) 20 J (c) 25 J (d) 30 J (e) 35 J

Fig. 28. Reflector-echo results for QI 16.

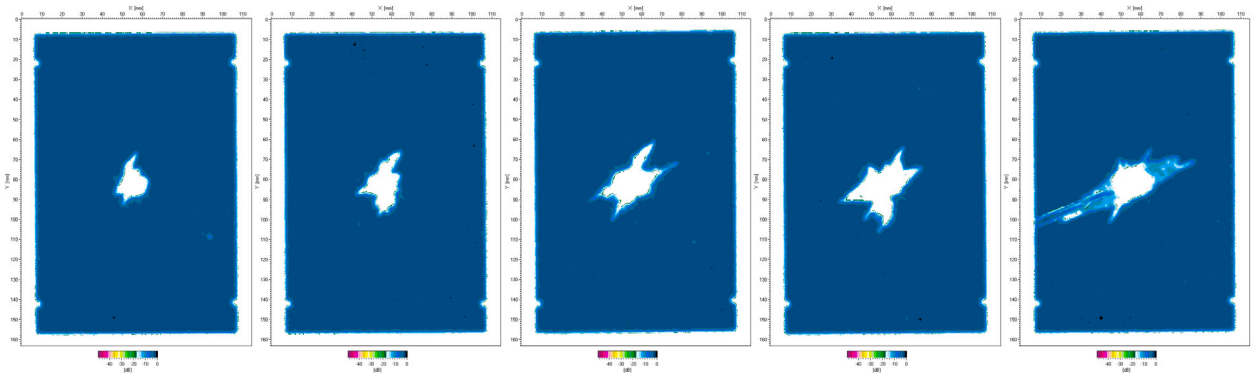

(a) 15 J (b) 20 J (c) 25 J (d) 30 J (e) 35 J

Fig. 29. Reflector-echo results for DD 16.

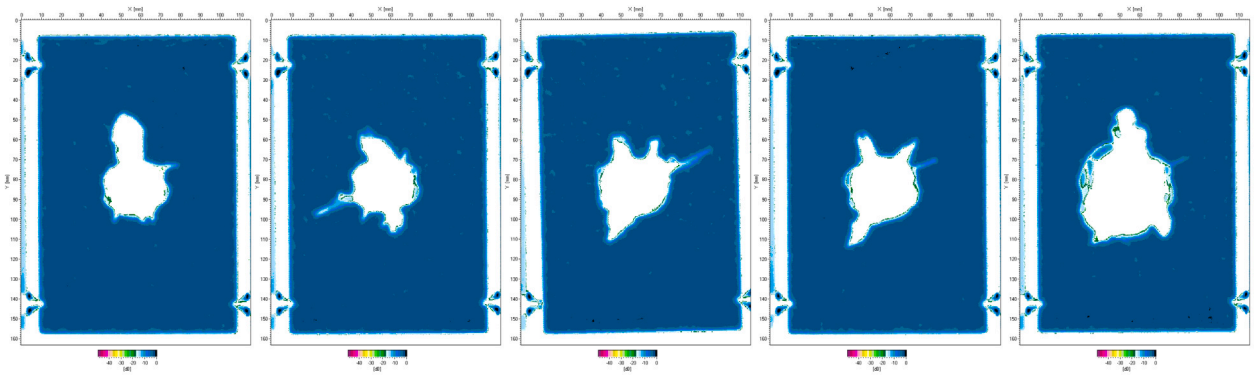

(a) 50 J (b) 55 J (c) 60 J (d) 65 J (e) 72 J

Fig. 30. Reflector-echo results for DD 32.

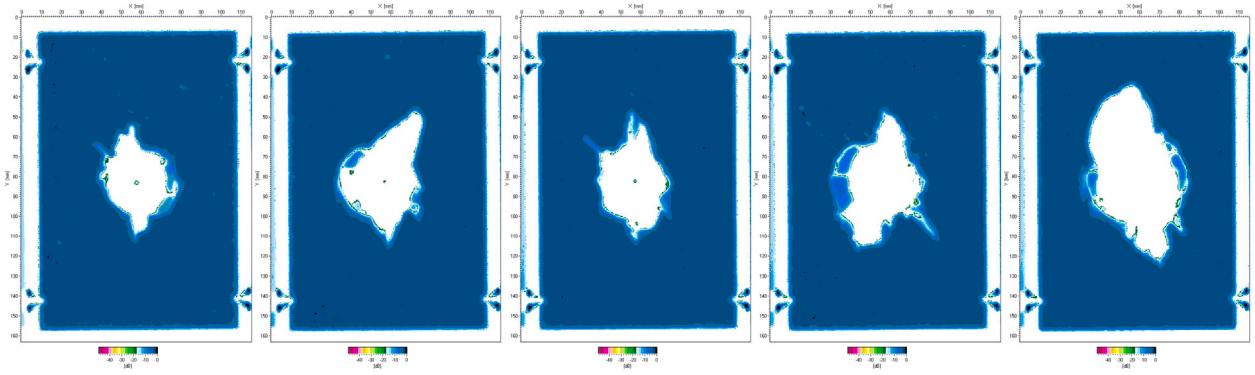

(a) 50 J (b) 55 J (c) 60 J (d) 65 J (e) 72 J

Fig. 31. Reflector-echo results for QI 32.

References

[1] S.W. Tsai, Double-double: New family of composite laminates, Am. Inst. Aeronaut. Astronaut. (AIAA) J. 59 (2021) 11.

[2] B. Vermes, S.W. Tsai, A. Riccio, F. Di Caprio, S. Roy, Application of the Tsai's modulus and double-double concepts to the definition of a new affordable design approach for composite laminates, Compos. Struct. 259 (2021) 113246.

[3] A. Garofano, A. Sellitto, V. Acanfora, F. Di Caprio, A. Riccio, On the effectiveness of double-double design on crashworthiness of fuselage barrel, Aerosp. Sci. Technol. 140 (2023) 108479.

[4] A.T. Nettles, Damage Tolerance of Composite Laminates from an Empirical Perspective, NASA, Marshall Space Flight Center, 2010.

[5] E. Kappel, Double-double laminates for aerospace applications - finding best laminates for given load sets, Composites Part C: Open Access 8 (2022) 100244.

[6] Airbus Test Method (AITM), Fibre reinforced plastics, Determ. Compression Strength After Impact, AITM1-0010 (3) (2005).

[7] X. Wang, J. Huang, R. Tan, Y. Su, Z. Guan, X. Gua, Experimental investigation on damage mechanisms and buckling behaviors of thin composite laminates in compression after impact, Compos. Struct. 256 (2021) 113122.

[8] M.A. Caminero, I. Garcia-Moreno, G.P. Rodriguez, Damage resistance of carbon fibre reinforced epoxy laminates subjected to low velocity impact: Effects of laminate thickness and ply-stacking sequence, Polym. Test. 63 (2017) 530–541.

[9] T. Garstka, Separation of Process Induced Distortions in Curved Composite Laminates (Ph.D. thesis), University of Bristol, UK, 2005.

[10] S. Rivallant, S. Bouvet, E.A. Abdallah, B. Broll, J.-J. Barrau, Experimental analysis of CFRP laminates subjected to compression after impact: The role of impact-induced cracks in failure, Compos. Struct. 111 (2014) 147–157.

[11] Y. Aoki, H. Samejima, H. Suemasu, Y. Nagao, Effect of Thickness on Impact Damage and CAI Behavior, ICCM, 2009.

[12] M. Duan, Z. Yue, Q. Song, Investigation of damage to thick composite laminates under low-velocity impact and frequency-sweep vibration loading conditions, Adv. Mech. Eng. 12 (10) (2020) 1–14.

[13] R.D.D. Cunha, T.G. Targino, C. Cardoso, E.P.D.C. Ferreira, R.C.S.F. Junior, J.D.D. Melo, Low velocity impact response of nontraditional double-double laminates, J. Compos. Mater. (2023).

[14] A. Baker, S. Dutton, D. Kelly, Composite Materials for Aircraft Structures, second ed., in: AIAA Education Series, 2004, p. 465.